

SN 2000cx and SN 2013bh: Extremely Rare, Nearly Twin Type Ia Supernovae

Jeffrey M. Silverman,^{1,2,3} Jozsef Vinko,^{1,4} Mansi M. Kasliwal,⁵ Ori D. Fox,⁶ Yi Cao,⁷ Joel Johansson,⁸ Daniel A. Perley,⁷ David Tal,⁹ J. Craig Wheeler,¹ Rahman Amanullah,⁸ Iair Arcavi,⁹ Joshua S. Bloom,⁶ Avishay Gal-Yam,⁹ Ariel Goobar,⁸ Shrinivas R. Kulkarni,⁷ Russ Laher,¹⁰ William H. Lee,¹¹ G. H. Marion,^{1,12} Peter E. Nugent,^{6,13} Isaac Shivvers⁶

¹*Department of Astronomy, University of Texas at Austin, Austin, TX 78712, USA*

²*NSF Astronomy and Astrophysics Postdoctoral Fellow*

³*email: jsilverman@astro.as.utexas.edu*

⁴*Department of Optics and Quantum Electronics, University of Szeged, Dóm tér 9, 6720 Szeged, Hungary*

⁵*Observatories of the Carnegie Institution of Science, Pasadena, CA 91101, USA*

⁶*Department of Astronomy, University of California, Berkeley, CA 94720-3411, USA*

⁷*Cahill Center for Astrophysics, California Institute of Technology, Pasadena, CA 91125, USA*

⁸*The Oskar Klein Centre, Department of Physics, AlbaNova, Stockholm University, SE-106 91 Stockholm, Sweden*

⁹*Benoziyo Center for Astrophysics, The Weizmann Institute of Science, Rehovot 76100, Israel*

¹⁰*Spitzer Science Center, California Institute of Technology, MC 314-6, Pasadena, CA 91125, USA*

¹¹*Instituto de Astronomía, Universidad Nacional Autónoma de México, Apartado Postal 70-264, 04510 México, D.F., México*

¹²*Harvard-Smithsonian Center for Astrophysics, 60 Garden St., Cambridge, MA 02138, USA*

¹³*Lawrence Berkeley National Laboratory, Berkeley, CA 94720, USA*

Accepted . Received ; in original form

ABSTRACT

The Type Ia supernova (SN Ia) SN 2000cx was one of the most peculiar transients ever discovered, with a rise to maximum brightness typical of a SN Ia, but a slower decline and a higher photospheric temperature. Thirteen years later SN 2013bh (aka iPTF13abc), a near identical twin, was discovered and we obtained optical and near-IR photometry and low-resolution optical spectroscopy from discovery until about 1 month past r -band maximum brightness. The spectra of both objects show iron-group elements (Co II, Ni II, Fe II, Fe III, and high-velocity features [HVF]s of Ti II), intermediate-mass elements (Si II, Si III, and S II), and separate normal velocity features (~ 12000 km s⁻¹) and HVFs (~ 24000 km s⁻¹) of Ca II. Persistent absorption from Fe III and Si III, along with the colour evolution, imply high blackbody temperatures for SNe 2013bh and 2000cx (~ 12000 K). Both objects lack narrow Na I D absorption and exploded in the outskirts of their hosts, indicating that the SN environments were relatively free of interstellar or circumstellar material and may imply that the progenitors came from a relatively old and low-metallicity stellar population. Models of SN 2000cx, seemingly applicable to SN 2013bh, imply the production of up to $\sim 1 M_{\odot}$ of ⁵⁶Ni and $(4.3\text{--}5.5) \times 10^{-3} M_{\odot}$ of fast-moving Ca ejecta.

Key words: supernovae: general – supernovae: individual (SN 2000cx, SN 2013bh)

1 INTRODUCTION

Resulting from the thermonuclear explosion of C/O white dwarfs (WDs; e.g., Nugent et al. 2011; Bloom et al. 2012), Type Ia supernovae (SNe Ia) provided the first clear indication that the expansion of the Universe is accelerating (Riess et al. 1998; Perlmutter et al. 1999) and have been used as precise distance indicators to accurately measure

cosmological parameters (e.g., Conley et al. 2011; Sullivan et al. 2011; Suzuki et al. 2012). Despite their utility, the specifics of SN Ia progenitor systems and explosion mechanisms are still unclear (see Howell 2011, for further information). In general, the two leading progenitor scenarios are the single-degenerate (SD) channel, when the WD accretes matter from a non-degenerate companion star (e.g., Whelan & Iben 1973), and the double-degenerate (DD) channel,

which is the result of the merger of two WDs (e.g., Iben & Tutukov 1984; Webbink 1984).

The ability to determine cosmological distances using SNe Ia lies mainly in the fact that they follow a light-curve decline rate versus peak luminosity correlation (i.e., the “Phillips relation”; Phillips 1993); however, the scatter in this relation is at least partially caused by the inclusion of various peculiar SNe Ia that nominally follow the correlation. Some of these objects, which are definitively classified as SNe Ia, can show extreme peculiarities. One of the most well-known and infamous of these objects is SN 2000cx.

SN 2000cx was discovered using the 0.76 m Katzman Automatic Imaging Telescope (KAIT; Richmond et al. 1993) on 2000 Jul. 17.5 (Yu et al. 2000, UT dates are used throughout), as part of the Lick Observatory Supernova Search (LOSS; Filippenko et al. 2001). It occurred in the outskirts of the nearby ($z = 0.00807$) S0 galaxy NGC 524 and was intensely observed by multiple groups (e.g. Li et al. 2001; Candia et al. 2003). It was soon discovered that SN 2000cx was peculiar in many ways. Its rise to maximum brightness in the B band was typical for a SN Ia, but it declined much slower than normal. Thus standard light curve fitting algorithms could not be reliably used on SN 2000cx (Li et al. 2001). Furthermore, the optical colours of the SN were redder than nearly all other SNe Ia near maximum brightness, but quickly became bluer than other SNe Ia by 15 d after maximum (Candia et al. 2003).

Spectroscopically, SN 2000cx showed strong Fe III and weak Si II and S II features, and thus resembled the over-luminous SN 1991T (Filippenko et al. 1992; Phillips et al. 1992). Unlike SN 1991T (and pretty much all other SNe Ia ever observed), SN 2000cx continued to show strong Fe III features (indicative of a high photospheric temperature) through 20 d past maximum brightness (Li et al. 2001). In addition, high-velocity features (HVFs) of Ca II were observed at velocities $> 20000 \text{ km s}^{-1}$, separated from a second set of Ca II features at more typical velocities ($\sim 12000 \text{ km s}^{-1}$, Thomas et al. 2004; Branch et al. 2004), the latter of which we will refer to as the photospheric velocity features (PVFs). These extreme observables indicate that SN 2000cx likely produced $> 0.5 M_{\odot}$ of ^{56}Ni (Sollerman et al. 2004) and possibly up to $\sim 1 M_{\odot}$ of ^{56}Ni (Li et al. 2001). SN 2000cx remained unique—until now.

Herein we present optical and near-IR photometry and low-resolution optical spectra of a near twin of SN 2000cx, SN 2013bh (aka iPTF13abc), during the first month after its discovery. We discuss the discovery of this object in §2 and present our observations and describe our data reduction in §3. Our analysis of the data, as well as a discussion of the host galaxy and possible progenitor system of SN 2013bh, can be found in §4. We summarize our conclusions in §5.

2 DISCOVERY

iPTF13abc was discovered on 2013 Mar. 23.5 with $r = 19.64 \pm 0.14$ mag as part of the intermediate Palomar Transient Factory (iPTF; Law et al. 2009; Rau et al. 2009; Kulkarni 2013). It was found at J2000.0 coordinates $\alpha = 15^{\text{h}}02^{\text{m}}13.09^{\text{s}}$, $\delta = +10^{\circ}38'45''.6$ in the star-forming galaxy SDSS J150214.17+103843.6 ($z = 0.0744$, Ahn et al. 2012). The field of iPTF13abc is shown in Figure 1 with the SN

Table 1. P48 Photometry of SN 2013bh

JD-2456000	R (mag)
366.88	<21.22
370.02	<21.46
375.02	19.70 (0.14)
376.03	19.43 (0.10)
377.01	19.22 (0.11)
386.98	18.35 (0.24)
392.95	18.49 (0.11)
393.78	18.50 (0.11)
396.94	18.80 (0.13)

1σ uncertainties are in parentheses.

marked with the green cross-hairs and a bright offset star marked with the red square. Up is north and left is east; the host galaxy of iPTF13abc is east and slightly south of the SN.

About 10 days later, this SN was independently discovered by the Catalina Real-Time Transient Survey (CRTS; Drake et al. 2009) as CSS130403:150213+103846, and upon public announcement of the discovery was christened SN 2013bh (Morales-Garoffolo et al. 2013). On 2013 Apr. 1.3, we obtained a spectrum of SN 2013bh and found that it was similar to the aforementioned SN 2000cx a few days before R -band maximum brightness. Three days later, the Public ESO Spectroscopic Survey of Transient Objects (PESSTO; e.g., Maund et al. 2013)¹ collaboration obtained a spectrum of this object and also found SN 2013bh to be spectroscopically similar to SN 2000cx (Drake et al. 2013).

3 OBSERVATIONS AND DATA REDUCTION

3.1 Photometry

SN 2013bh was discovered using the 48 in Samuel Oschin Telescope at Palomar Observatory (P48). Every night since 15 May 2013, P48 observed the field of SN 2013bh three times in the R -band,² weather-permitting. Adjacent visits were separated by at least 45 min. The P48 images of SN 2013bh were processed with the iPTF LBL pipeline (Nugent et al. in preparation). Aperture photometry was then performed on each of these images with an aperture radius equal to the seeing of each image. Aperture correction coefficients were calculated by measuring unsaturated stars that have signal-to-noise ratio (S/N) > 20 with two apertures, one of which had a radius of seeing while the other had a radius of three times seeing. Relative photometry was done among all P48 images while the absolute photometry was calibrated to r -band data of the Sloan Digital Sky Survey (SDSS) Data Release 9 (DR9) Catalogue (Ahn et al. 2012). The P48 R -band data of SN 2013bh is presented in Table 1.

After discovery, multiple telescopes were employed in

¹ <http://www.pessto.org/pessto/index.py>

² All photometric data presented herein are in AB mags, except the J - and H -band data which are in Vega mags.

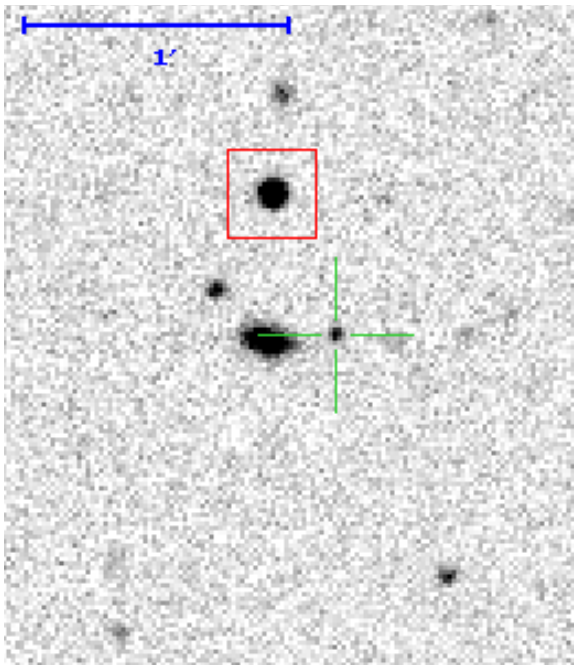


Figure 1. The field of iPTF13abc with the SN marked with the green cross-hairs and a bright offset star marked with the red square. Up is north and left is east. The host galaxy of iPTF13abc is east and slightly south of the SN.

order to follow SN 2013bh photometrically. As part of regular iPTF operations (Law et al. 2009), robotic multi-band (*gr_i*) follow-up photometry was obtained with the Palomar 60 in (P60). First, the images were reduced using the automated P60 pipeline (Cenko et al. 2006). Next, calibration star magnitudes were measured on the best seeing image. Finally, aperture photometry on SN 2013bh was undertaken (with the radius equal to the seeing and the background annulus equal to 3 and 5 times the seeing) and calibrated relative to these stars. Given the offset from the host galaxy, image subtraction was not required. Table 2 shows our P60 photometry of SN 2013bh.

Using ALFOSC at the Nordic Optical Telescope (NOT), La Palma, we obtained *BVRI* photometry of SN 2013bh. All data have been reduced with standard IRAF³ routines, using the QUBA pipeline (see Valenti et al. 2011, for more information). The magnitudes are measured with aperture photometry (with the radius equal to the 2 times the seeing and the background annulus equal to 3 and 5 times the seeing) and calibrated to the Landolt system through observations of standard stars PG1047+003 and PG1525-071. In order to match the other SN 2013bh photometry, the *RI* data from NOT were converted to *ri* magnitudes using the conversions presented by Jordi et al. (2006). These data are presented in Table 3.

Optical and near-IR photometry (*riZYJH*) were obtained with the multi-channel Reionization And Transients InfraRed camera (RATIR; Butler et al. 2012) mounted on

Table 2. P60 Photometry of SN 2013bh

JD-2456000	<i>g</i> (mag)	<i>r</i> (mag)	<i>i</i> (mag)
375.40	...	19.42 (0.05)	...
388.44	18.38 (0.02)	18.31 (0.03)	18.94 (0.06)
389.34	18.41 (0.03)	18.31 (0.03)	18.93 (0.05)
390.25	18.44 (0.05)	18.34 (0.04)	19.14 (0.11)
392.21	18.53 (0.06)	18.36 (0.05)	19.10 (0.12)
393.21	...	18.46 (0.02)	19.08 (0.05)
406.17	...	19.39 (0.14)	...
409.19	20.11 (0.42)	19.33 (0.11)	...
412.42	20.18 (0.08)	19.50 (0.05)	19.89 (0.09)
413.41	19.85 (0.07)
414.31	20.32 (0.06)
415.32	19.91 (0.08)
416.22	20.54 (0.06)	19.60 (0.08)	...
417.36	19.95 (0.15)
422.38	21.06 (0.08)	20.17 (0.06)	20.39 (0.11)
423.36	21.11 (0.10)	20.20 (0.06)	20.38 (0.10)
426.22	21.13 (0.10)	20.32 (0.06)	20.51 (0.11)
427.21	21.26 (0.15)	20.43 (0.08)	20.62 (0.15)

1σ uncertainties are in parentheses.

the 1.5 m Johnson telescope at the Mexican Observatorio Astronómico Nacional on Sierra San Pedro Mártir in Baja California, México (Watson et al. 2012). Typical observations include a series of 60 s exposures in *riZYJH*, with dithering between exposures. The fixed IR filters of RATIR cover half of their respective detectors, automatically providing off-target IR sky exposures while the target is observed in the neighboring filter. Master IR sky frames are created from a median stack of off-target images in each IR filter. No off-target sky frames were obtained on the opti-

³ IRAF: The Image Reduction and Analysis Facility is distributed by the National Optical Astronomy Observatory, which is operated by the Association of Universities for Research in Astronomy (AURA) under cooperative agreement with the National Science Foundation (NSF).

Table 4. RATIR Photometry of SN 2013bh

JD-2456000	r (mag)	i (mag)	Z (mag)	Y (mag)	J (mag)	H (mag)
386.00	18.34 (0.01)	18.88 (0.01)	...	19.15 (0.05)	...	<18.50
389.00	18.26 (0.01)	18.93 (0.01)	...	19.39 (0.05)	...	<18.50
397.00	18.61 (0.03)	19.66 (0.03)
398.00	18.64 (0.01)	19.56 (0.02)	...	19.95 (0.11)	...	<18.50
399.00	18.77 (0.01)	19.73 (0.02)	19.98 (0.07)	19.93 (0.12)	<19.40	<18.50
410.00	...	19.88 (0.02)	20.45 (0.10)	19.73 (0.06)	<19.90	<18.50
423.00	20.30 (0.02)	20.25 (0.03)	20.65 (0.12)	20.02 (0.11)	<19.30	<18.50

1σ uncertainties are in parentheses.

Table 6. Journal of Spectroscopic Observations of SN 2013bh

UT Date	Epoch ^a	Instrument	Range (Å)	Res. (Å) ^b	Exposure (s)
2013 Apr. 1.31	-3.6	LRS	4192-10204	15.6	2000
2013 Apr. 5.40	0.2	EFOOSC2	3764-9283	18	1500
2013 Apr. 6.46	1.2	LRS	4192-10128	15.4	2000
2013 Apr. 9.56	4.1	LRIS	3764-10204	4.5/6	480
2013 Apr. 11.44	5.8	LRS	4192-10204	15.5	2000
2013 Apr. 13.48	7.7	DBSP	3624-9872	3/4	300
2013 Apr. 16.43	10.5	LRS	4192-10204	15.2	2000
2013 Apr. 22.26	15.9	LRS	4204-10204	15.6	2000
2013 Apr. 27.23	20.5	LRS	4288-10200	15.9	2500

^aRest-frame days relative to the date of r -band maximum (2013 Apr. 5.2).
^bLRS = Low-Resolution Spectrograph on the 9.2 m Hobby-Eberly Telescope at McDonald Observatory; EFOOSC2 = ESO Faint Object Spectrograph and Camera v.2 on the NTT; LRIS = Low Resolution Imaging Spectrometer on the 10 m Keck I telescope; DBSP = Double Spectrograph on the Palomar 200 in telescope.
^bApproximate full width at half-maximum intensity (FWHM) resolution. If two numbers are listed, they represent the blue- and red-side resolutions, respectively.

the light curve of SN 2013bh is slightly broader than that of SN 2000cx.

Given $E(B - V)_{\text{MW}} = 0.0284$ mag (Schlegel et al. 1998), no reddening from the host galaxy of SN 2013bh (see Section 4.3), and $\mu = 37.57 \pm 0.15$ mag (see Section 4.6), the peak absolute magnitudes of SN 2013bh in our best observed bands are $M_r = -19.3 \pm 0.15$ mag and $M_i = -18.7 \pm 0.34$ mag. These values are in agreement with those of SN 2000cx, after correcting for $E(B - V)_{\text{MW}} = 0.08$ mag and no host reddening (-19.24 and -18.94 , respectively; Li et al. 2001).

4.1.1 The B and V Bands

While we do not have data on the rising portion of the B -band light curve of SN 2013bh, we note that SN 2000cx was found to have a similar rise time to that of the normal Type Ia SN 1994D (Li et al. 2001). Based on two data points, SN 2013bh has a slightly slower decline than SN 2000cx in the B band (much like the r and i bands, see below), but has a very similar V -band light curve. SN 2000cx was found to have a normal B -band decline rate until 6 d after B -band maximum brightness, after which time the decline slowed (Li et al. 2001).

4.1.2 The r Band

The best observed bandpass of SN 2013bh is the r band, and in Figure 3 we present its r -band light curve, along with data from various comparison objects: SN 2000cx (solid; Li et al. 2001), the overluminous type Ia SN 1991T (dotted; Lira et al. 1998), and the normal type Ia SN 2011fe (dashed; Vinkó et al. 2012). All comparison objects have had their published R -band data converted to r -band magnitudes using the conversions in Jordi et al. (2006) and have been deredshifted and dereddened by values given in their respective references. The top panel of Figure 3 shows absolute r -band magnitudes while the bottom panel is the same data, but shifted such that all objects have the same peak magnitude.

Once again, the light curve of SN 2013bh matches well to that of SN 2000cx and both are slightly more luminous at peak (in the r -band) than SN 2011fe, but less luminous than SN 1991T. The r -band is the only band for which we have pre-maximum data of SN 2013bh. Based on these observations, it appears that SN 2013bh has a relatively normal rise time, similar to that of SN 2000cx.

The r band of SN 2013bh shows a plateau that begins between 12 and 17 d after r -band maximum brightness, similar to SN 2000cx for which the plateau begins at ~ 15 d after maximum, which is later than more normal SNe Ia (~ 12 d

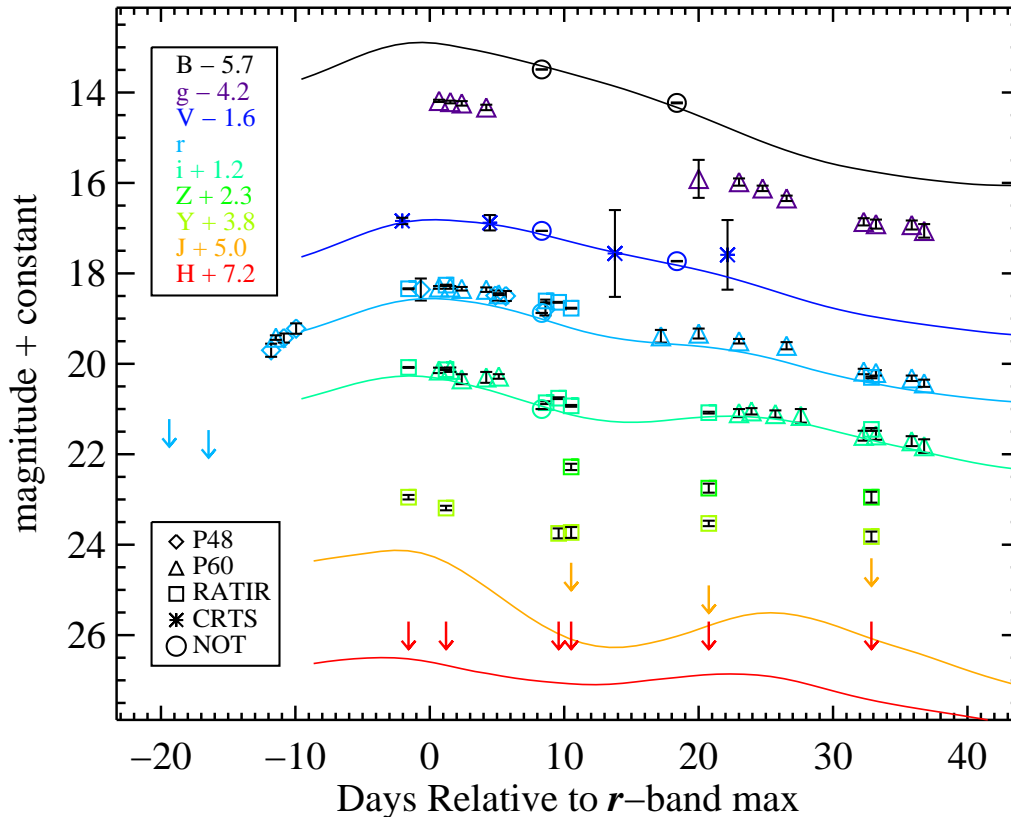


Figure 2. *BgVriZYJH* light curves of SN 2013bh (points), compared with those of SN 2000cx (solid lines, Li et al. 2001; Candia et al. 2003). The SN 2000cx data has been shifted in time to match the *r*-band peak of SN 2013bh and shifted in apparent magnitude to the distance of SN 2013bh. Neither of the objects have been dereddened.

for SN 1994D and ~ 14 d for SN 2011fe, Li et al. 2001; Vinkó et al. 2012, respectively). Since the plateau begins later and the secondary *r*-band maximum is weaker in SNe 2013bh and 2000cx than in other SNe Ia, the amount these objects have faded shortly after maximum brightness is larger than that of the comparison objects shown in Figure 3. As mentioned above, SN 2013bh has a slightly slower *r*-band decline rate after maximum brightness than SN 2000cx, but it is clear that both are faster than the other objects in the Figure. Finally, the *r*-band plateau in SN 2013bh ends between 23 and 27 d past maximum, again similar to SN 2000cx.

4.1.3 The *iZYJH* Bands

The *i*-band data of SN 2000cx was normal until about 7 d after *r*-band maximum brightness at which time it began to decline faster than normal SNe Ia. At 14 d past maximum it had faded ~ 1.1 mag below peak after which it re-brightened somewhat (Li et al. 2001). It is likely that SN 2013bh also behaved this way, but unfortunately, we do not have *i*-band data at this epoch. We do see evidence, however, that SN 2013bh (like SN 2000cx) has a weak secondary maximum, as compared to more normal SNe Ia, in the *i* band (just like the *r* band). These secondary maxima are usually associated with Fe III recombining to form Fe II as the SN ejecta cools (Pinto & Eastman 2000a). Weak sec-

ondary maxima indicate that the SN photosphere remains relatively hot through these epochs, which is consistent with the blackbody temperatures and strong Fe III absorptions seen in SN 2013bh at these epochs (see Section 4.4).

Moving further into the IR, the *Z* and *Y* data of SN 2013bh also show weak secondary maxima as compared to other SNe Ia, which is similar to the weak secondary maxima in *JHK* data of SN 2000cx (Candia et al. 2003). SN 2000cx, and many other SNe Ia, have been found to have $M_H \approx -17.9$ mag at 10 d after *B*-band maximum (Candia et al. 2003), which is consistent with our observed upper limit of $M_H > -18.9$ mag at this epoch. Furthermore, Candia et al. (2003) observed a deep dip in the *J*-band light curve of SN 2000cx at about 13 d past maximum brightness and this is certainly consistent with our upper limits for SN 2013bh.

4.2 Colour Curves

In Figure 4 we plot the colour evolution of SN 2013bh, along with the same comparison objects that were shown in Figure 3. As above, all objects have been corrected for Galactic extinction using the dust maps of Schlegel et al. (1998) and information in their respective references.

The *B* – *V* colour of SN 2013bh is redder than all of the comparison objects at ~ 8 d after *r*-band maximum bright-

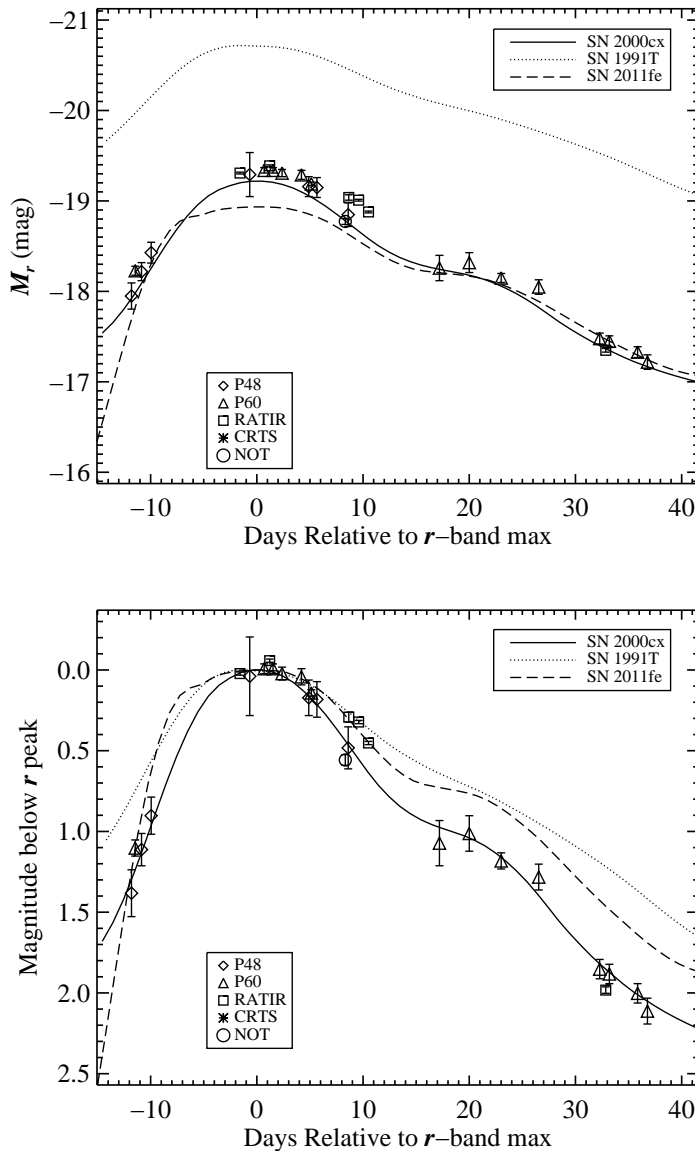


Figure 3. The r -band light curve of SN 2013bh with some comparison objects: SN 2000cx (solid; Li et al. 2001), the overluminous type Ia SN 1991T (dotted; Lira et al. 1998), and the normal type Ia SN 2011fe (dashed; Vinkó et al. 2012). All R -band photometry has been converted to r -band magnitudes using conversions found in Jordi et al. (2006). All data have been deredshifted and dereddened by values given in their respective references. Absolute r -band magnitudes are shown (*top*) as well as a shifted version of the data such that all objects have the same peak magnitude (*bottom*).

ness, but then becomes nearly as blue as SN 2000cx by ~ 18 d after maximum. The $B - V$ colour of SN 2000cx was also seen to be quite red at early times, becoming extremely blue by 2 weeks after maximum. This was due to a plateau in the colour curve at $B - V = 0.3$ mag for $6 < t < 15$ d (Li et al. 2001; Candia et al. 2003). Even though SN 2013bh data are sparse, the observations are consistent with a plateau at $B - V \approx 0.4 - 0.5$ mag at similar epochs as the one seen in SN 2000cx, though perhaps a bit later.

The single $V - R$ observation of SN 2013bh from ~ 8 d after maximum brightness is slightly redder than the $V - R$ colour of SN 2000cx at the same epoch. SN 2000cx (and presumably SN 2013bh as well) is bluer than normal and overluminous SNe Ia at all epochs studied herein and shows

a deep blue dip at ~ 12 d after maximum (as seen in the upper-right panel of Figure 4 and Li et al. 2001). In $V - I$ it was also seen that SN 2000cx was bluer than other SNe Ia and again showed a deep blue dip, though in this colour the dip is a few days earlier than in $V - R$. We see a similar behavior in our one $V - I$ data point for SN 2013bh, though it is significantly (~ 0.3 mag) bluer than even SN 2000cx.

The $r - i$ colours of SN 2013bh, for which we have a handful of data points, are found to match SN 2000cx near r -band maximum brightness. Soon after maximum, however, SN 2013bh evolves to be bluer than SN 2000cx in $r - i$. The minimum in the $r - i$ colour curve of SN 2013bh occurs at ~ 9 d after maximum and is about 0.2 mag bluer than that of SN 2000cx. At later epochs, SN 2013bh remains \sim

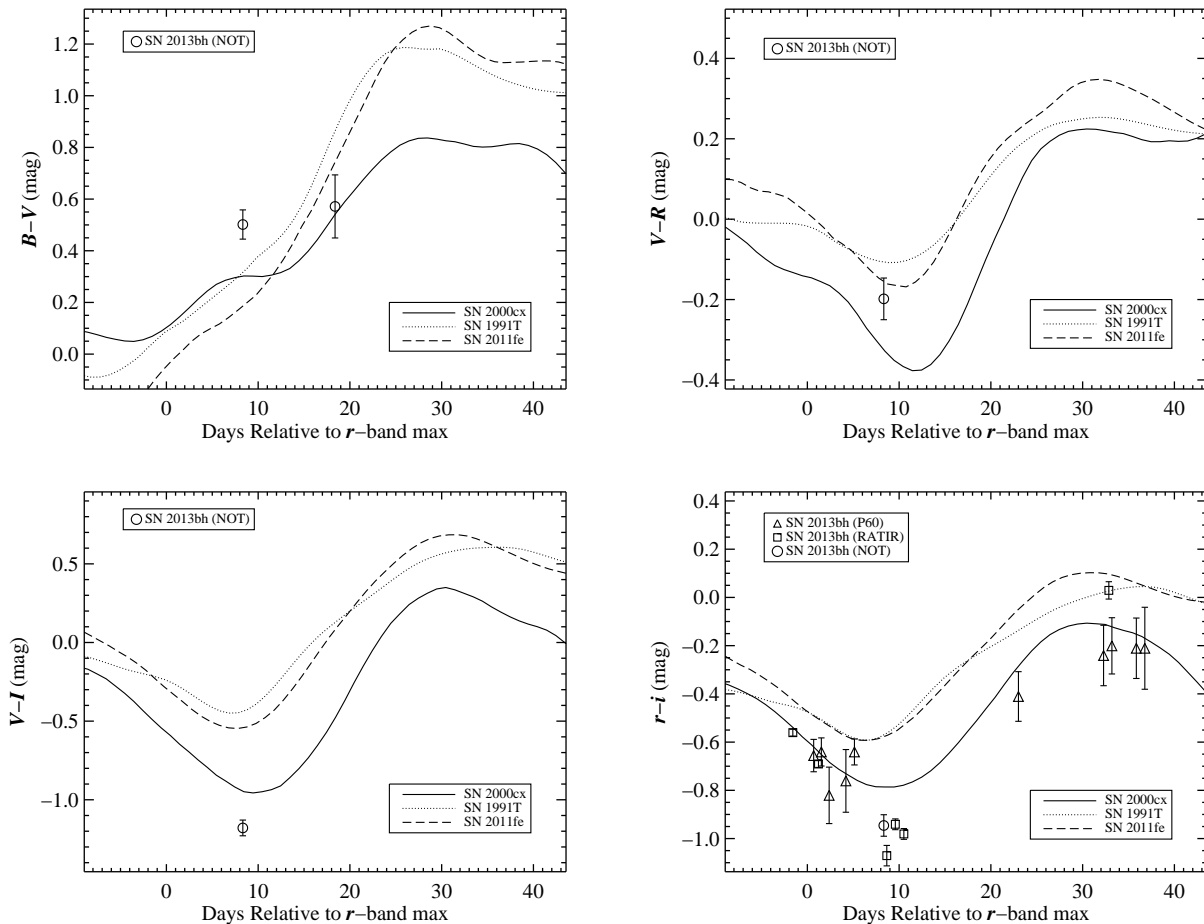


Figure 4. Colour curves of SN 2013bh and the same comparison objects used in Figure 3. All data have been deredshifted and corrected for extinction using the reddening values provided in their respective references.

0.1 mag bluer than SN 2000cx. Note that the majority of the difference in $r-i$ of SN 2013bh at about 1 month past maximum as measured from P60 and RATIR data comes from the i -band photometry, though it is still consistent at about the 2σ level. Furthermore, no instrumental response corrections have been applied to our data and, as mentioned above, no host-galaxy subtraction was performed.

In summary, based on limited data, the colours of SN 2013bh tend to follow those of SN 2000cx, and certainly more closely than either SN 1991T or SN 2011fe. However, SN 2013bh appears to have more extreme colours than SN 2000cx. In general SN 2013bh seems to be redder than SN 2000cx in the bluest colours, but bluer than SN 2000cx in the reddest bands. This implies an optical continuum that peaks redder than SN 2000cx, thus SN 2013bh seems to have a lower blackbody temperature which is consistent with our spectral models (see Section 4.4).

4.3 Spectra

All of our spectra of SN 2013bh are shown in black in Figure 5 and are labelled with their age relative to r -band maximum brightness. The over-plotted red, dashed curves are spectra of SN 2000cx at similar epochs to our observations

of SN 2013bh, also labelled by their age relative to r -band maximum brightness (converted from the date of R -band maximum brightness as determined by Li et al. 2001). The SN 2000cx comparison data come from the in-depth study of that object by Li et al. (2001) and the large CfA SN Ia spectral dataset presented by Matheson et al. (2008). Both objects have been deredshifted and dereddened. The spectral match between SN 2013bh and SN 2000cx at all epochs studied in this work is remarkable. We do note, however, that SN 2000cx seems to have a slightly bluer continuum than SN 2013bh, which is indicative of a higher blackbody temperature, once again consistent with our spectral models (see Section 4.4).

We assumed above no reddening from the host galaxy of SN 2013bh. This is due mainly to the facts that we see no evidence of absorption from Na I D and because it was found in the outskirts of its host (much like SN 2000cx). In our highest S/N spectrum from 4 d after r -band maximum brightness, we find a 2σ upper limit of 0.2 \AA for the equivalent width (EW) of Na I D absorption. Using the empirical relation of Poznanski et al. (2011), this converts to $E(B-V)_{\text{host}} < 0.006$ mag, which is negligible (especially given the uncertainties in the conversion, i.e. ~ 0.3 mag). Also supporting no host reddening is the location of SN 2013bh in its host galaxy. It went off ~ 24 kpc (projected linear

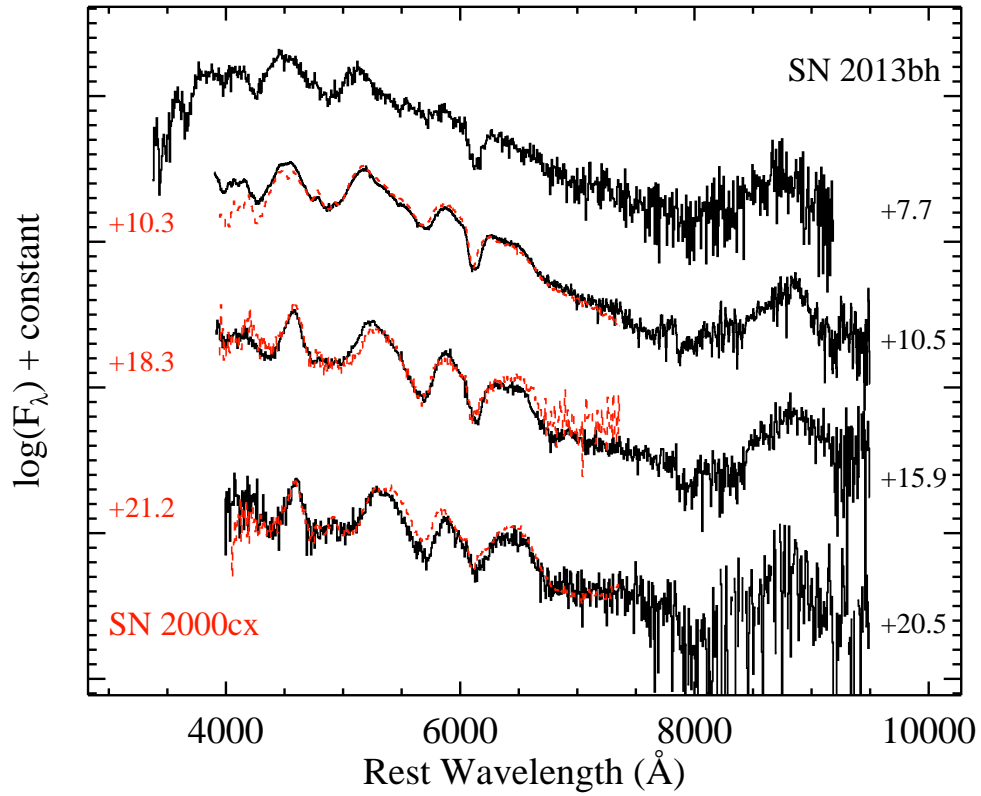
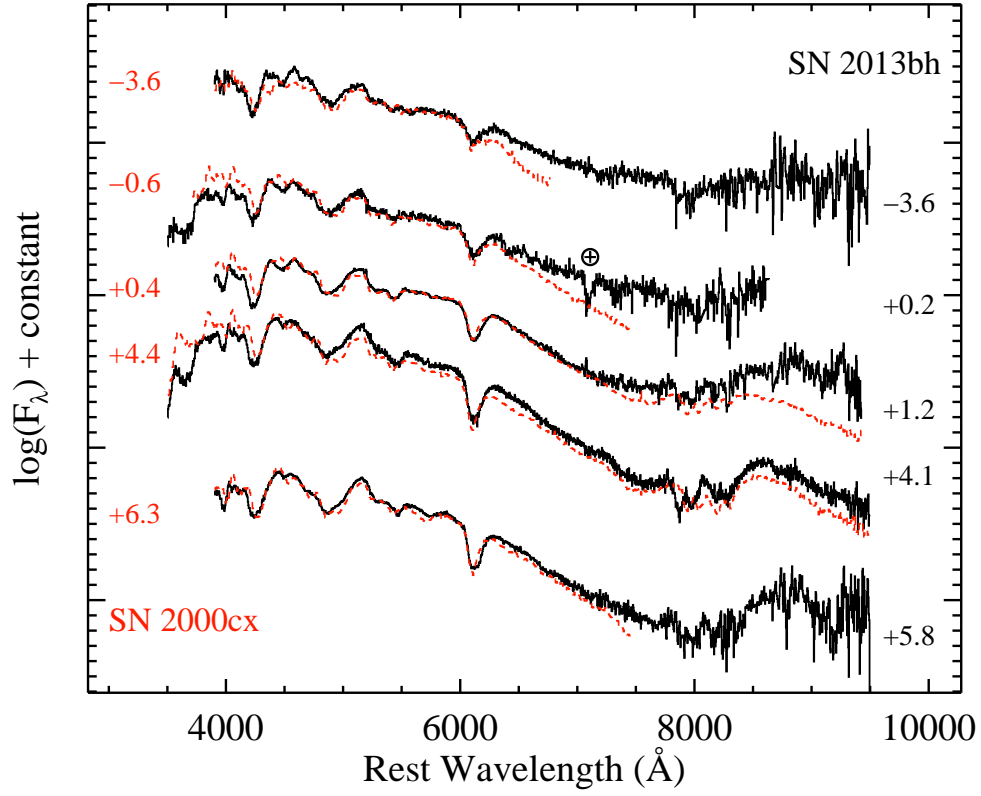


Figure 5. Spectra of SN 2013bh (solid black) and SN 2000cx (dashed red, taken from Li et al. 2001; Matheson et al. 2008), both labelled with their age relative to r -band maximum brightness. Telluric absorption in the maximum light spectrum is marked by the Earth symbol (\oplus) and both objects have been deredshifted and dereddened.

distance) from the centre of SDSS J150214.17+103843.6, which is equivalent to ~ 3 Petrosian radii (Petrosian 1976). See Section 4.6 for more information on the host galaxy of SN 2013bh.

In Figure 6 we compare our highest S/N spectrum of SN 2013bh (from ~ 4 d past maximum brightness) with various other SNe Ia at similar epochs. Shown in the Figure are its near twin, SN 2000cx (Li et al. 2001), as well as the overluminous SN 1991T (Filippenko et al. 1992) and the extremely normal SN 2011fe (Parrent et al. 2012). Important spectral features are labelled. SN 2011fe stands out from the other three objects with overall much stronger absorption features and a much broader and more blended Ca II near-IR triplet. Further differences are seen in the blue end of the spectrum where SN 2011fe is dominated by absorption from blends of Fe II and Mg II lines, while the complex profiles in the other objects are due in large part to Fe III and Ti II (see §4.4 for further information).

Even though SNe 2013bh and 2000cx bear some resemblance to SN 1991T, there are significant differences as well. The O I line is more prominent in SN 1991T than in either SNe 2013bh and 2000cx, where it is almost non-existent. This (along with a lack of C absorption) may be an indication of more complete WD burning in SNe 2013bh and 2000cx, which is consistent with the relatively large amount of ^{56}Ni inferred for these objects (see § 4.6). SNe 2013bh and 2000cx both also show significant absorption from HVFs of Ti II while SN 1991T lacks these features in the blue end of the spectrum. In addition, just blueward of the Ca II near-IR triplet in these latter two objects, a second absorption component from HVFs of Ca II is easily seen and is conspicuously absent from SN 1991T.

4.4 Spectral Fits

The spectrum-synthesis code *SYNAPPS* (Thomas et al. 2011) was employed to help identify the species present in our spectra of SN 2013bh. *SYNAPPS* (and its modeling kernel *SYN++*) is derived from *SYNOW* (Fisher et al. 1997), which computes synthetic spectra of SNe in the photospheric phase using the Sobolev approximation (Sobolev 1960; Castor 1970; Jeffery 1989). *SYNAPPS* is capable of varying a large number of parameters automatically, thus finding an optimum fit via χ^2 -minimization.

In *SYNAPPS* models the spectral lines are assumed to form via resonance scattering above a sharp photosphere. The location of the photosphere is expressed in velocity coordinates as v_{ph} (in km s^{-1}) taking into account the homologous expansion of the SN ejecta. Consequently, for a particular ion, the minimum and maximum velocity coordinates of the line-forming region are denoted with v_{min} and v_{max} (both in km s^{-1}), respectively. If $v_{\text{min}} \gtrsim v_{\text{ph}}$, then the line forming region is considered “detached” from the photosphere.

The optical depths for each transition of a given species are controlled with two additional parameters: the optical depth of a “reference line,” τ_{ref} (which is usually the strongest line in the optical band, defined internally within the code), and the e-folding width, v_e (in km s^{-1}), of the optical depth profile above the photosphere (assumed to be an exponential function in *SYNAPPS*). For other features, the op-

tical depth is computed relative to the reference line assuming Boltzmann-excitation (i.e. local thermodynamic equilibrium) using an excitation temperature T_{exc} (in K). Non-LTE effects are mimicked partly by allowing different T_{exc} values for each species, all of which can be different from the photospheric temperature T_{phot} . The latter is used only in computing the blackbody radiation emitted by the photosphere. Since the number of species appearing in a typical SN spectrum is usually between 5 and 10, and each ion has 5 tunable parameters, the number of adjustable parameters in a *SYNAPPS* session can be substantial.

The spectral sequence of SN 2013bh in Figure 5 suggests that the optical spectra shortly before and after maximum brightness are formed by the same set of ions, and the spectral evolution can be modeled by simply tuning the optical depth and other parameters of the same species. This is supported by the similar photospheric temperature of the pre-maximum and post-maximum spectra, which suggests that the excitation of ions should not change drastically near maximum.

A model containing the usual composition of a SN Ia was constructed to fit the spectra of SN 2013bh and is based on the model for SN 2000cx by Branch et al. (2004) and Thomas et al. (2004). The model was initially fit to the 4.1 d spectrum, then it was optimized for the -3.6 and $+6.3$ d spectra. *SYNAPPS* fits to these three SN 2013bh spectra are shown in Figure 7. The data are shown as solid black, while the models are shown as dashed red. Major spectral features have been labelled. The parameters of our *SYNAPPS* fit to the 4.1 d spectrum are listed in Table 7.

The model includes PVFs of Ca II, Si II, S II, Fe III, Co II, and Ni II, in addition to detached, HVFs of Ca II, Si III, Ti II, and Fe II. The photospheric velocity is $v_{\text{ph}} \approx 11000 \text{ km s}^{-1}$ for all modeled spectra and the detached, HVFs span a range between 20000 and 24000 km s^{-1} . These modeled velocities are fully consistent with what is calculated from direct measurements of the spectral features themselves (§ 4.5), including a Si II velocity plateau seen in our SN Ia-like *SYNAPPS* fits. From Figure 7, it is clear that most of the spectral features between 3000 and 6300 Å can be fit successfully with the models. As also seen in other, more normal SNe Ia at similar epochs (e.g., Silverman et al. 2012a), redward of ~ 6300 Å, the continuum is significantly depressed relative to the blackbody continuum, which cannot be modeled self-consistently within the framework of *SYNAPPS*. Therefore, this region has been omitted from the automatic fitting process.

We identify Ca II via the near-IR triplet (at ~ 8000 Å) as well as Ca II H&K (at ~ 3650 Å). The strong, unblended feature near 6150 Å is due to Si II $\lambda 6355$ and the feature near 5480 Å is from S II. The model is able to fit the observed feature near 4000 Å, which was identified in SN 2000cx as a blended HVF from Ti II by Branch et al. (2004) and could also be due to Si II $\lambda 4130$, despite the presence of these ions in our model. Note that the feature at 4500 Å, suspected to be a HVF of H β in SN 2000cx by Branch et al. (2004), can be fit adequately as a blend of iron-group elements.

As mentioned above, our *SYNAPPS* model of SN 2013bh is extremely similar to models of SN 2000cx. Li et al. (2001) found that Si II $\lambda 6355$ strengthened with time in SN 2000cx while Fe III remained strong through maximum brightness,

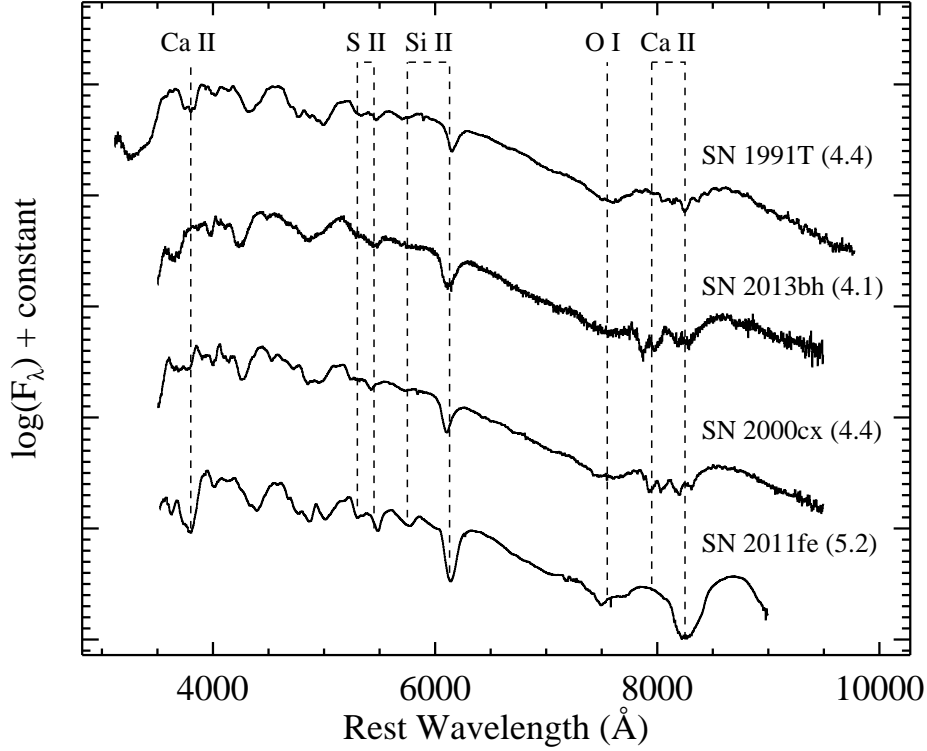


Figure 6. A spectrum of SN 2013bh along with comparisons to other SNe Ia: SN 1991T (Filippenko et al. 1992), SN 2000cx (Li et al. 2001), and SN 2011fe (Parrent et al. 2012). Each spectrum is labelled with its age relative to r/R -band maximum brightness and the data have all been deredshifted and dereddened. Significant spectral features have been identified.

Table 7. SYNAPPS Model Parameters for the 4.1 d Spectrum

Ion	$\log \tau_{\text{ref}}$	v_{min} (10^3 km s^{-1})	v_{max} (10^3 km s^{-1})	v_e (10^3 km s^{-1})	T_{exc} (10^3 K)
Si II	1.57	12.0	40.0	1.0	8.8
Si III	1.34	16.0	40.0	2.0	13.0
S II	-2.00	12.0	40.0	1.0	5.2
Ca II (PVF)	0.80	12.0	40.0	4.8	12.0
Ca II (HVF)	2.90	25.0	40.0	3.0	12.0
Ti II	2.09	21.0	40.0	2.0	5.5
Fe II	0.94	21.2	40.0	4.0	5.0
Fe III	0.03	11.0	40.0	2.0	12.0
Co II	0.60	11.0	40.0	2.0	6.3
Ni II	1.00	11.0	40.0	2.0	5.1

$v_{\text{ph}} = 11000 \text{ km s}^{-1}$, $T_{\text{phot}} = 11000 \text{ K}$.

which is identical to what we find for SN 2013bh. S II was found to be weak in both objects, but vanished quicker in SN 2013bh than SN 2000cx. HVFs of Fe II occurred in both objects, but we find evidence of only PVFs for Fe III and Si II while SN 2000cx showed evidence for HVFs of these ions (Li et al. 2001; Thomas et al. 2004). Evidence for O I and Mg II absorption in SN 2000cx was presented by Thomas et al. (2004) and Branch et al. (2004), respectively, though our SYNAPPS fits do not support the same claim for SN 2013bh. Models in both of those studies do indicate Ca II velocities

in SN 2000cx that match what we find for SN 2013bh quite well. In addition, Branch et al. (2004) note significant absorption due to HVFs of Ti II in their models of SN 2000cx and we find similar results for our models of SN 2013bh.

For epochs studied herein, the photospheric temperatures inferred from our SYNAPPS fits to SN 2013bh are $\sim 11000 \text{ K}$. This is higher than more normal SNe Ia, though slightly cooler than what was found for SN 2000cx (12000 K ; Thomas et al. 2004). Note, however, that at slightly earlier epochs (about 1 week before maximum brightness), a much

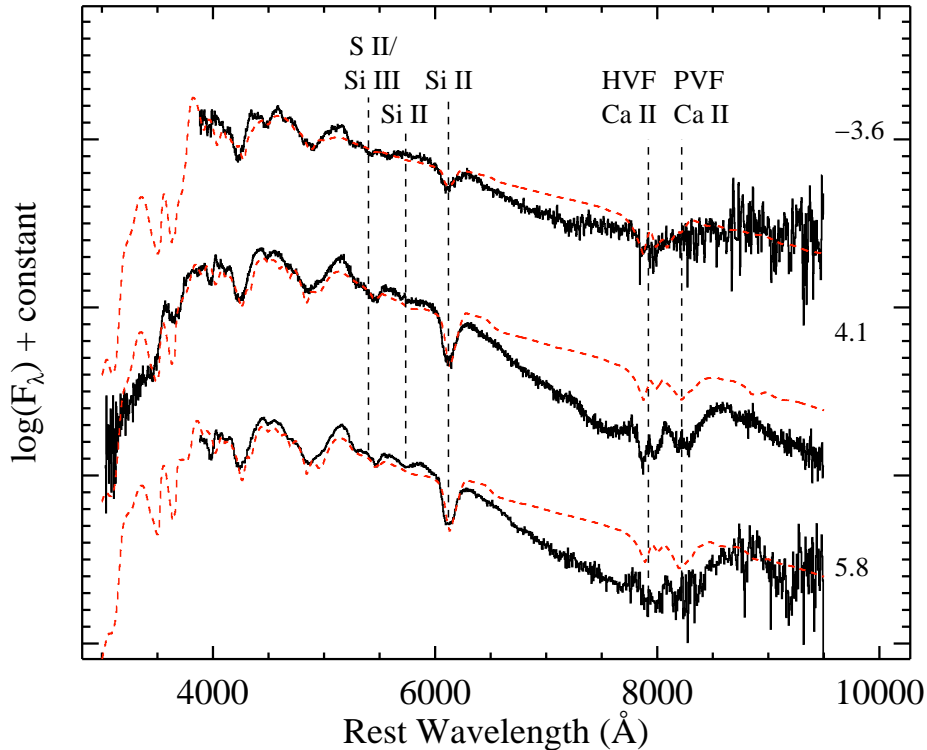


Figure 7. Observed spectra of SN 2013bh (solid black) and SYNAPPS fits to the data (dashed red). Each spectrum is labelled with its age relative to r -band maximum brightness and the data have all been deredshifted and dereddened. Major spectral features are identified.

higher blackbody temperature for SN 2000cx was inferred from near-IR spectra (20000-25000 K; Rudy et al. 2002).

4.5 Expansion Velocities

For a few of the spectral features in SN 2013bh (and SN 2000cx) which are easily-identifiable and relatively well-separated, the expansion velocities are measured. Here we investigate the Si II $\lambda 6355$ feature, the S II “W” feature,⁷ the Ca II H&K feature, and the Ca II near-IR triplet. For the Si II and S II features, the method of velocity determination is the same as that used in Silverman et al. (2012), but, briefly, consists of: defining two endpoints on either side of the feature of interest, fitting a linear pseudo-continuum between those endpoints, fitting a spline function to the data between the endpoints, and using the minimum of the spline fit to calculate an expansion velocity for the feature.

For the Ca II features, however, we employed a slightly different fitting method. Similar to the method outlined above, we begin by choosing endpoints for the spectral feature in question and, using these endpoints, define and then subtract from the data a linear pseudo-continuum. Then a non-linear least squares fitter is used to simultaneously fit

multiple Gaussian components to each component of the feature. The Ca II H&K feature (Ca II near-IR triplet) consists of 2 (3) distinct components. Given that the relative fluxes (set by the gf weights) and rest wavelengths of each component are known and since we require that all components in a given fit have the same Gaussian width, each Ca II fit contains only 3 free parameters: the Gaussian height, width, and centroid of the strongest component. By-eye initial estimates of these parameters for each fit are used as inputs to the fitting routine.

For the Ca II H&K profile, we also allow for the existence of absorption due to Si II $\lambda 3858$ at a similar velocity to Si II $\lambda 6355$ (e.g., Foley 2012). We find that Si II $\lambda 3858$ is extremely weak (or non-existent) in our spectra of SN 2013bh that cover this wavelength range. We do, however, find evidence for Si II $\lambda 3858$ absorption in SN 2000cx at velocities consistent with Si II $\lambda 6355$.

All of the measured velocities for SN 2013bh are consistent with our SYNAPPS fits and are plotted in Figure 8 (*filled black*), relative to r -band maximum brightness. We also plot (*open grey*) our re-measured velocities of SN 2000cx (also relative to r -band maximum) using spectra presented in Li et al. (2001) and Matheson et al. (2008). Note that the velocities for SN 2000cx calculated herein are consistent with previous work (Li et al. 2001; Thomas et al. 2004; Branch et al. 2004).

The upper panel of Figure 8 shows the velocities of the Si II $\lambda 6355$ and S II “W” features for SNe 2013bh and 2000cx, along with the 1σ region (*light grey*) around the av-

⁷ The two broad absorptions that make up the S II “W” are fit using a single spline, but we calculate the expansion velocity of the absorption complex using the minimum of the bluer of the two features relative to its rest wavelength.

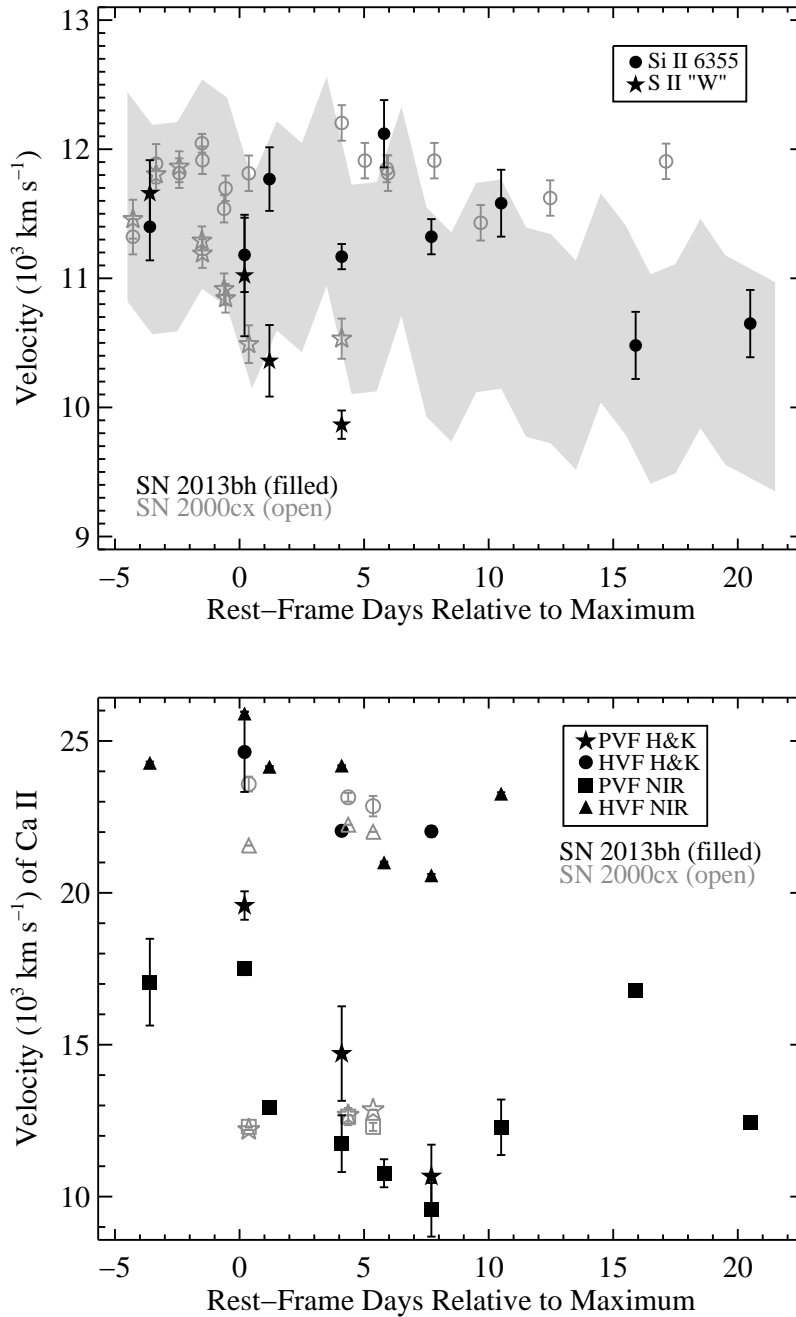


Figure 8. The temporal evolution of the expansion velocities (relative to r -band maximum brightness) of SN 2013bh (*filled black*) and SN 2000cx (*open grey*). The top panel shows velocities of the Si II $\lambda 6355$ (*circles*) and S II “W” features (*stars*). The bottom panel shows velocities of PVFs and HVFs of Ca II H&K (*stars* and *circles*, respectively) and PVFs and HVFs of the Ca II near-IR triplet (*squares* and *triangles*, respectively). The light grey swath in the top panel is the 1σ region around the average Si II $\lambda 6355$ velocity of normal SNe Ia as determined by the entire BSNIP dataset. Note that the HVFs and PVFs of the Ca II near-IR triplet in SN 2013bh become blended by 16 d after maximum brightness and thus are shown as a single (black filled square) data point from then on.

average Si II $\lambda 6355$ velocity of normal SNe Ia as determined by the entire Berkeley SN Ia Program sample (BSNIP; Silverman et al. 2012). The Si II $\lambda 6355$ velocity of SN 2013bh is initially similar to other, more normal SNe Ia, but shows a plateau until ~ 10 d after maximum brightness, thus becoming larger than the typical SN Ia Si II $\lambda 6355$ velocity. After this epoch, the velocity decreases some, eventually matching

the more normal SNe Ia. SN 2000cx also shows a plateau at nearly the same velocity (~ 11500 – 12000 km s^{-1}) though it is much longer lived, lasting through all epochs for which we measure a Si II $\lambda 6355$ velocity in this work. In fact, Li et al. (2001) found that this plateau continues to $t > 40$ d. Such long-lasting Si II velocity plateaus are not unheard of, though all other examples of them are found in extremely

peculiar SNe Ia (e.g., Scalzo et al. 2010; Childress et al. 2013).

The width of the Si II $\lambda 6355$ feature in SN 2013bh is larger than that of SN 2000cx, but we do not see any convincing evidence for HVFs from Si II, even though this has been seen in other SNe Ia (e.g., Silverman et al. 2012b; Childress et al. 2013; Marion et al. 2013). In both SNe 2000cx and 2013bh, the Si II $\lambda 6355$ and S II “W” features both strengthen with time, though while the former stays strong through all epochs considered here, the latter begins to weaken after maximum brightness and completely disappears by a few days after maximum.

As seen in Figure 5, the S II “W” feature is somewhat weaker in SN 2013bh as compared to SN 2000cx near maximum brightness. This spectral feature is usually found to have velocities 1000-2000 km s⁻¹ lower than the Si II $\lambda 6355$ feature (e.g., Silverman et al. 2012), though in SNe 2013bh and 2000cx both features have similar velocities before maximum. At this point the velocity plummets, likely due to the feature getting progressively weaker and becoming blended with other ions (notably Si III, see § 4.4).

The spectra of SN 2000cx blueward of the Ca II near-IR triplet were initially found to be quite complex and confusing (Li et al. 2001), but it was eventually realized, through spectral modeling, that this object showed HVFs of Ca II at velocities > 20000 km s⁻¹ (Thomas et al. 2004; Branch et al. 2004). This was in addition to a second set of Ca II features at more typical velocities (~ 12000 km s⁻¹). HVFs from Ca II have been seen in many individual SNe Ia (e.g., Silverman et al. 2012b; Childress et al. 2013; Marion et al. 2013) and might be common in the early-time spectra of SNe Ia (e.g., Mazzali et al. 2005; Childress et al. 2013; Silverman et al. in preparation). Unsurprisingly, SN 2013bh once again matches SN 2000cx and shows strong HVFs from Ca II at early times.

The bottom panel of Figure 8 shows the velocities for SN 2013bh (*filled black*) and SN 2000cx (*open grey*) of PVFs and HVFs of Ca II H&K (*stars* and *circles*, respectively) and PVFs and HVFs of the Ca II near-IR triplet (*squares* and *triangles*, respectively). In both objects, through ~ 10 d past maximum, we measure distinct PVFs and HVFs for both the Ca II H&K feature and the Ca II near-IR triplet. The PVF velocities are similar to more normal SNe Ia at these epochs, while the HVF velocities of both objects are significantly larger than most SNe Ia (Childress et al. 2013; Silverman et al. in preparation). By 16 d past maximum, we are only able to measure a single Ca II near-IR triplet feature in SN 2013bh. Since the measured velocity at this epoch is nearly the average of the HVF and PVF velocities from the previous spectrum, it appears that the two components have become blended and thus are shown in the Figure as a single (black filled square) data point from then on.

The measured velocities of the PVFs for both Ca II features in SN 2000cx are nearly identical, while the HVF velocities of this objects also match each other quite well. This is a useful sanity check for our velocity determinations since one might expect all Ca II features in a given spectrum to have nearly equal velocities. The velocities of the PVFs and HVFs are quite self-consistent for SN 2013bh as well. Also note the relatively small scatter in *all* PVF velocity measurements (both objects and both spectral features), as well as the consistency of all of the HVF velocity measure-

ments. This once again emphasizes the similarity between these two objects.

To highlight the separation between the HVFs and the PVFs, as well as our multiple Gaussian component fitting technique, we plot the full Ca II near-IR triplet profile for SNe 2013bh (*top*) and 2000cx (*bottom*) in Figure 9. Both spectra were obtained ~ 4 d after maximum and have had their linear pseudo-continua (grey dotted line) removed. The data are the black curves, the combined Gaussian fits are the grey solid curves, and the individual Gaussian components are the grey short-dashed curves. The separation between the HVFs (left-hand triplet of Gaussians) and the PVFs (right-hand triplet of Gaussians) can easily be seen in both objects. While we fully admit that the fits are not perfect and fitting a set of Gaussians to the full profile is an oversimplification, they do appear to capture the overall shapes of both profiles, as well as at least some of the more subtle details. The fits tend to have reduced χ^2 values of 2-3.

The vertical solid line is the Ca II near-IR triplet velocity for SN 2013bh, while the vertical long-dashed line is the velocity for SN 2000cx. The PVFs in these two objects have consistent expansion velocities at this epoch, however the HVFs of SN 2013bh are found to be at larger velocities than those of SN 2000cx (which can also be seen in Figure 8). Perhaps this indicates a higher Ca II optical depth in SN 2013bh. A more detailed analysis of HVFs is beyond the scope of this paper, but an in-depth study of HVFs in a large set of more normal SN Ia spectra will be undertaken in the near future (Silverman et al. in preparation).

4.6 Host Galaxy and Progenitor System

SN 2013bh lies in the outskirts of the star-forming galaxy SDSS J150214.17+103843.6 at a redshift of $z = 0.0744$ (Ahn et al. 2012), which, assuming a Λ CDM cosmology with $H_0 = 73$ km s⁻¹ Mpc⁻¹, implies a distance of 326 ± 22 Mpc and a distance modulus of $\mu = 37.57 \pm 0.15$ mag. It is located $15'9''$ west and $2'0''$ north of the centre of its host, a projected distance of ~ 25.3 kpc (or ~ 3 Petrosian radii, Petrosian 1976). Correlation with a library of galaxy spectra using the “SuperNova IDentification” code (SNID; Blondin & Tonry 2007) indicates that SDSS J150214.17+103843.6 is a spiral (Sa/Sb) galaxy with $z = 0.075$, quite close to the SDSS DR9 value of $z = 0.0744$ (Ahn et al. 2012). While this is not an atypical type of host galaxy for a SN Ia (Li et al. 2011), very few (if any) SNe Ia are found further away from the centre of their host (e.g., Wang et al. 2013).

While inner parts of the host galaxy of SN 2013bh may be currently forming stars, the outer edges (where the SN is located) show no obvious *u*-band emission (Ahn et al. 2012), indicating a lack of star formation ($\lesssim 4.9 \times 10^{-2}$ M_⊙ yr⁻¹; e.g., ?). In addition, typical metallicity gradients in spiral galaxies (e.g., Henry & Worthey 1999) indicate that SN 2013bh went off in a region that likely has relatively low-metallicity.

SN 2000cx also exploded in the periphery of its host galaxy, the nearby (~ 38 Mpc) S0 galaxy NGC 524. It was found 18 kpc (linear projected distance) from the centre of its host, in a low-metallicity region (Li et al. 2001). High-resolution spectra of SN 2000cx presented by Patat et al. (2007) do not show evidence of Na I D absorption to very tight limits and they infer $N(\text{Na I}) \leq 2 \times 10^{10}$ cm⁻² and

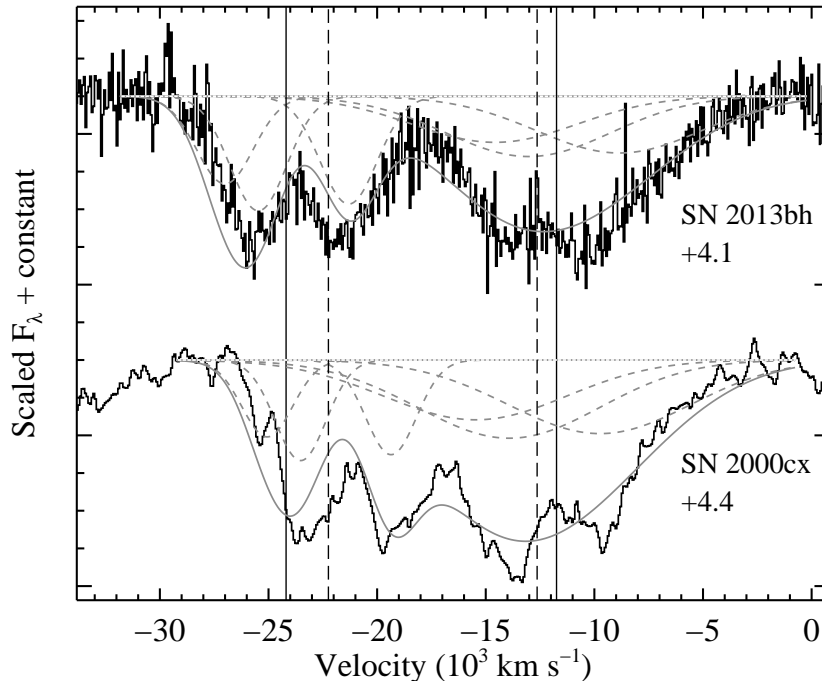


Figure 9. The Ca II near-IR triplet profile for SNe 2013bh (*top*) and 2000cx (*bottom*), after removing the linear pseudo-continuum (grey dotted line). The rest-frame age of each spectrum is listed next to the data (*black*). Over-plotted are the combined Gaussian fits (*solid grey*) and the individual Gaussian components (*short-dashed grey*). The HVFs are the left-side Gaussians while the PVFs are the right-side Gaussians. The Ca II near-IR triplet velocity of SN 2013bh (SN 2000cx) is shown as the vertical solid (long-dashed) line.

(for solar abundances) $N(\text{H}) \leq 3 \times 10^{16} \text{ cm}^{-2}$. As mentioned above, our highest S/N spectrum of SN 2013bh also did not show obvious absorption from Na I D (with a 2σ upper limit of 0.2 \AA) or evidence for star formation from narrow emission lines.

Both SN 2013bh and SN 2000cx lack Na I D absorption which indicates low host-galaxy reddening and a relatively “clean” circumstellar environment (i.e., free of expelled material from the companion star). Their locations on the periphery of their host galaxies, along with no obvious associated recent star formation, point to old stellar population progenitors with relatively low-metallicity for both objects. All of these observations are consistent with many DD models (e.g., Iben & Tutukov 1984), though we cannot definitively rule out all SD models (e.g., Whelan & Iben 1973).

Li et al. (2001) and Candia et al. (2003) found that none of the standard SN Ia light-curve fitting algorithms could match the observations of SN 2000cx, and thus the same can be said for SN 2013bh; however, the delayed-detonation DD3 model (Woosley & Weaver 1994; Pinto & Eastman 2000b) did match many of the observations of SN 2000cx. This model produced higher kinetic energies and more nuclear burning than models of more normal SNe Ia (including the overluminous SN 1991T). As a result, the DD3 model produced a relatively large amount of ^{56}Ni ($\sim 1 M_{\odot}$), higher-than-normal blackbody temperatures, and high expansion velocities. The latter two observables were seen in both SN 2000cx (Li et al. 2001; Thomas et al. 2004; Branch et al. 2004) and SN 2013bh (Sections 4.4 and 4.5). Furthermore,

this model also predicted peak magnitudes and Δm_{15} values consistent with those observed for both SN 2000cx and SN 2013bh.

An alternative explanation for the HVFs observed in these two objects comes from a 3D model presented by Thomas et al. (2004). They explain the HVFs of Ca II as coming from clumpy ejecta such that the high-velocity material only partially covers the SN photosphere. This idea is supported by Leonard et al. (2000), who found significant polarization intrinsic SN 2000cx. Thomas et al. (2004) also derive $(4.3\text{--}5.5) \times 10^{-3} M_{\odot}$ for the high-velocity ejecta mass in Ca, which they claim can be explained by primordial material alone. This conclusion is consistent with the “clean” environment determined for SNe 2000cx and 2013bh by the lack of Na I D or narrow Ca II H&K absorption from circumstellar material.

5 CONCLUSIONS

In this work we have presented optical and near-IR photometry of SN 2013bh (aka iPTF13abc), a near twin of SN 2000cx, from discovery through ~ 40 d past r -band maximum brightness and low-resolution optical spectroscopy through ~ 20 d past maximum. SN 2013bh reached a peak absolute magnitude of $M_r = -19.2$ mag and had a decline rate of $\Delta m_{15}(r) = 0.73$ mag, matching nearly identically to SN 2000cx. The colours of SN 2013bh mostly follow those of SN 2000cx, but show evidence of a slightly “flatter” optical continuum that indicates a slightly lower blackbody

temperature than SN 2000cx. This is consistent with the relative spectral shapes of these two objects. The colours of SNe 2000cx and 2013bh also indicate photospheric temperatures that are higher than more normal SNe Ia. This is supported by the presence of strong absorption features from Fe III and Si III that persist well past maximum brightness (which is not seen in any other SN Ia). Our spectral models from SYNAPPS and direct measurements of the strongest spectral features also indicate the presence of other iron-group elements (Co II, Ni II, Fe II, and HVFs of Ti II) and intermediate-mass elements (Si II and S II). Furthermore, in all of our spectra we observe separate normal velocity features ($\sim 12000 \text{ km s}^{-1}$) and HVFs ($\sim 24000 \text{ km s}^{-1}$) of Ca II.

The environments of both SN 2013bh and SN 2000cx appear to be relatively “clean,” with negligible amounts of CSM, consistent with their locations in the outskirts of their host galaxies and the lack of obvious associated recent star formation. This points to the progenitors of these objects being relatively low-metallicity, old stars, consistent with the DD scenario (though the SD scenario cannot be completely disproved). The delayed-detonation DD3 model of Woosley & Weaver (1994); Pinto & Eastman (2000b) was successfully applied to SN 2000cx and given the observational similarities with SN 2013bh, it is reasonable to use it for this object as well. This model implies a relatively large amount of ^{56}Ni produced ($\sim 1 M_{\odot}$), higher-than-normal blackbody temperatures, and high expansion velocities. The latter two of these were directly observed in SN 2013bh. The model also predicts peak magnitudes and Δm_{15} values consistent with those observed for both SN 2000cx and SN 2013bh. A 3D model presented by Thomas et al. (2004) explains the HVFs of Ca II as coming from $(4.3\text{--}5.5) \times 10^{-3} M_{\odot}$ of clumpy ejecta, which can be explained by primordial material alone.

Of the ~ 2300 SNe Ia given IAU designations from the beginning of 2000 through the end of 2012, SN 2000cx was the only one of its kind discovered. PTF, which ran for 4 years starting in 2009, discovered 1250 SNe Ia with no objects resembling SN 2000cx. iPTF, which began in Jan 2013, discovered SN 2013bh (aka iPTF13abc) and through the end of Jul 2013 has found 111 SNe Ia. Very roughly, it seems that an object like SN 2000cx or SN 2013bh is found in every ~ 2000 SNe Ia. In other words, these objects are approximately 0.05% of the total SN Ia rate. The extreme rarity of these objects and how they relate to more normal SNe Ia and overluminous SN 1991T-like objects is a challenge to SN progenitor models. As large-scale transient surveys (e.g., iPTF, Pan-STARRS, LSST) continue to (and will in the future) find many new objects, more objects similar to SNe 2000cx and 2013bh will likely be discovered.

ACKNOWLEDGMENTS

We would like to thank M. Ganeshalingam, P. Kelly, and E. Ofek for helpful discussions, J. Caldwell, S. Odewahn, and S. Rostopchin for their assistance with some of the observations, as well as the PESSTO and CRTS collaborations for making some of their data on SN 2013bh publicly available. The HET is a joint project of the University of Texas at Austin, the Pennsylvania State University, Stanford University, Ludwig-Maximilians-Universität München, and Georg-

August-Universität Göttingen. The HET is named in honor of its principal benefactors, William P. Hobby and Robert E. Eberly. The Marcario Low Resolution Spectrograph is named for Mike Marcario of High Lonesome Optics who fabricated several optics for the instrument but died before its completion. The LRS is a joint project of the HET partnership and the Instituto de Astronomía de la Universidad Nacional Autónoma de México. Some of the data presented herein were obtained at the W. M. Keck Observatory, which is operated as a scientific partnership among the California Institute of Technology, the University of California, and the National Aeronautics and Space Administration (NASA); the observatory was made possible by the generous financial support of the W. M. Keck Foundation. The authors wish to recognize and acknowledge the very significant cultural role and reverence that the summit of Mauna Kea has always had within the indigenous Hawaiian community; we are most fortunate to have the opportunity to conduct observations from this mountain. This work is partially based on observations made with the Nordic Optical Telescope, operated on the island of La Palma jointly by Denmark, Finland, Iceland, Norway, and Sweden, in the Spanish Observatorio del Roque de los Muchachos of the Instituto de Astrofísica de Canarias. We thank the RATIR instrument team and the staff of the Observatorio Astronómico Nacional on Sierra San Pedro Mártir. RATIR is a collaboration between the University of California, the Universidad Nacional Autónoma de México, NASA Goddard Space Flight Center, and Arizona State University, benefiting from the loan of an H2RG detector from Teledyne Scientific and Imaging. RATIR, the automation of the Harold L. Johnson Telescope of the Observatorio Astronómico Nacional on Sierra San Pedro Mártir, and the operation of both are funded by the partner institutions and through NASA grants NNX09AH71G, NNX09AT02G, NNX10AI27G, and NNX12AE66G, CONACyT grants INFR-2009-01-122785, UNAM PAPIIT grant IN113810, and a UC MEXUS-CONACyT grant. The National Energy Research Scientific Computing Center, supported by the Office of Science of the U.S. Department of Energy, provided staff, computational resources, and data storage for this project. This research has made use of the NASA/IPAC Extragalactic Database (NED) which is operated by the Jet Propulsion Laboratory, California Institute of Technology, under contract with NASA. Funding for SDSS-III has been provided by the Alfred P. Sloan Foundation, the Participating Institutions, the NSF, and the U.S. Department of Energy Office of Science. The SDSS-III web site is <http://www.sdss3.org/>. JMS is supported by an NSF Astronomy and Astrophysics Postdoctoral Fellowship under award AST-1302771. JV is supported by Hungarian OTKA Grant NN 107637. MMK acknowledges generous support from the Hubble Fellowship and Carnegie-Princeton Fellowship. JCW’s supernova group at UT Austin is supported by NSF Grant AST 11-09801. Some work on this paper by JCW was done in the hospitable clime of the Aspen Center for Physics that is supported by NSF Grant PHY-1066293. JSB acknowledges the generous support of a CDI grant (#0941742) from the National Science Foundation.

REFERENCES

- Ahn C. P., et al., 2012, *ApJS*, 203, 21
- Blondin S., Tonry J. L., 2007, *ApJ*, 666, 1024
- Bloom J. S., et al., 2012, *ApJ*, 744, L17
- Branch D., et al., 2004, *ApJ*, 606, 413
- Butler N., et al., 2012, in *Society of Photo-Optical Instrumentation Engineers (SPIE) Conference Series Vol. 8446 of Society of Photo-Optical Instrumentation Engineers (SPIE) Conference Series, First Light with RATIR: An Automated 6-band Optical/NIR Imaging Camera*. p. 34
- Buzzoni B., et al., 1984, *The Messenger*, 38, 9
- Candia P., et al., 2003, *PASP*, 115, 277
- Castor J. I., 1970, *MNRAS*, 149, 111
- Cenko S. B., et al., 2006, *PASP*, 118, 1396
- Childress M. J., et al., 2013, *ApJ*, 770, 29
- Childress M. J., Filippenko A. V., Ganeshalingam M., Schmidt B. P., 2013, *MNRAS*, submitted (arXiv:1307.0563)
- Conley A., et al., 2011, *ApJS*, 192, 1
- Drake A. J., et al., 2009, *ApJ*, 696, 870
- Drake A. J., et al., 2013, *Central Bureau Electronic Telegrams*, 3480, 1
- Filippenko A. V., et al., 1992, *ApJ*, 384, L15
- Filippenko A. V., Li W. D., Treffers R. R., Modjaz M., 2001, in *Paczynski B., Chen W. P., Lemme C., eds, Small-Telescope Astronomy on Global Scales. Vol. 246, The Lick Observatory Supernova Search with the Katzman Automatic Imaging Telescope*. *Astron. Soc. Pac.*, San Francisco, p. 121
- Fisher A., Branch D., Nugent P., Baron E., 1997, *ApJ*, 481, L89
- Foley R. J., 2012, *MNRAS*, submitted (arXiv:1212.6261)
- Foley R. J., et al., 2003, *PASP*, 115, 1220
- Fox O. D., et al., 2012, in *Society of Photo-Optical Instrumentation Engineers (SPIE) Conference Series Vol. 8453 of Society of Photo-Optical Instrumentation Engineers (SPIE) Conference Series, Performance and calibration of H2RG detectors and SIDECAR ASICs for the RATIR camera*. p. 59
- Fox O. D., Filippenko A. V., 2013, *ApJ*, in press (arXiv:1304.4934)
- Henry R. B. C., Worthey G., 1999, *PASP*, 111, 919
- Hill G. J., et al., 1998, in *D'Odorico S., ed., Society of Photo-Optical Instrumentation Engineers (SPIE) Conference Series Vol. 3355 of Society of Photo-Optical Instrumentation Engineers (SPIE) Conference Series, Hobby-Eberly Telescope low-resolution spectrograph: mechanical design*. pp 433–443
- Howell D. A., 2011, *Nature Communications*, 2, 350
- Howell D. A., et al., 2006, *Nature*, 443, 308
- Iben Jr. I., Tutukov A. V., 1984, *ApJS*, 54, 335
- Jeffery D. J., 1989, *ApJS*, 71, 951
- Jordi K., Grebel E. K., Ammon K., 2006, *A&A*, 460, 339
- Kasliwal M. M., et al., 2012, *ApJ*, 755, 161
- Kulkarni S. R., 2013, *The Astronomer's Telegram*, 4807, 1
- Law N. M., et al., 2009, *PASP*, 121, 1395
- Leonard D. C., Filippenko A. V., Chornock R., Li W. D., 2000, *IAU Circ.*, 7471, 3
- Li W., et al., 2001, *PASP*, 113, 1178
- Li W., et al., 2011, *MNRAS*, 412, 1473
- Lira P., et al., 1998, *AJ*, 115, 234
- Marion G. H., et al., 2013, *ApJ*, submitted (arXiv:1302.3537)
- Matheson T., et al., 2008, *AJ*, 135, 1598
- Matheson T., Filippenko A. V., Ho L. C., Barth A. J., Leonard D. C., 2000, *AJ*, 120, 1499
- Maund J. R., et al., 2013, *MNRAS*, 431, L102
- Mazzali P. A., et al., 2005, *ApJ*, 623, L37
- Morales-Garoffolo A., et al., 2013, *The Astronomer's Telegram*, 4955, 1
- Nugent P. E., et al., 2011, *Nature*, 480, 344
- Oke J. B., Cohen J. G., Carr M., et al., 1995, *PASP*, 107, 375
- Oke J. B., Gunn J. E., 1982, *PASP*, 94, 586
- Parrent J. T., et al., 2012, *ApJ*, 752, L26
- Patat F., et al., 2007, *Science*, 317, 924
- Perlmutter S., et al., 1999, *ApJ*, 517, 565
- Petrosian V., 1976, *ApJ*, 209, L1
- Phillips M. M., 1993, *ApJ*, 413, L105
- Phillips M. M., Wells L. A., Suntzeff N. B., Hamuy M., Leibundgut B., Kirshner R. P., Foltz C. B., 1992, *AJ*, 103, 1632
- Pinto P. A., Eastman R. G., 2000a, *ApJ*, 530, 757
- Pinto P. A., Eastman R. G., 2000b, *ApJ*, submitted (arXiv:000.6171)
- Poznanski D., Ganeshalingam M., Silverman J. M., Filippenko A. V., 2011, *MNRAS*, 415, L81
- Rau A., et al., 2009, *PASP*, 121, 1334
- Richmond M., Treffers R. R., Filippenko A. V., 1993, *PASP*, 105, 1164
- Riess A. G., et al., 1998, *AJ*, 116, 1009
- Rudy R. J., Lynch D. K., Mazuk S., Venturini C. C., Puetter R. C., Höflich P., 2002, *ApJ*, 565, 413
- Scalzo R. A., et al., 2010, *ApJ*, 713, 1073
- Schlegel D. J., Finkbeiner D. P., Davis M., 1998, *ApJ*, 500, 525
- Silverman J. M., et al., 2012a, *MNRAS*, 425, 1789
- Silverman J. M., et al., 2012b, *ApJ*, 756, L7
- Silverman J. M., et al., 2013, *ApJS*, accepted (arXiv:1303.0763)
- Silverman J. M., Ganeshalingam M., Li W., Filippenko A. V., Miller A. A., Poznanski D., 2011, *MNRAS*, 410, 585
- Silverman J. M., Kong J. J., Filippenko A. V., 2012, *MNRAS*, 425, 1819
- Skrutskie M. F., et al., 2006, *AJ*, 131, 1163
- Sobolev V. V., 1960, *Moving envelopes of stars*. Cambridge: Harvard University Press
- Sollerman J., et al., 2004, *A&A*, 428, 555
- Sullivan M., et al., 2011, *ApJ*, 737, 102
- Suzuki N., et al., 2012, *ApJ*, 746, 85
- Thomas R. C., Branch D., Baron E., Nomoto K., Li W., Filippenko A. V., 2004, *ApJ*, 601, 1019
- Thomas R. C., Nugent P. E., Meza J. C., 2011, *PASP*, 123, 237
- Valenti S., et al., 2011, *MNRAS*, 416, 3138
- Vinkó J., et al., 2012, *A&A*, 546, A12
- Wade R. A., Horne K., 1988, *ApJ*, 324, 411
- Wang X., Wang L., Filippenko A. V., Zhang T., Zhao X., 2013, *Science*, 340, 170
- Watson A. M., et al., 2012, in *Society of Photo-Optical Instrumentation Engineers (SPIE) Conference Series Vol. 8444 of Society of Photo-Optical Instrumentation*

Engineers (SPIE) Conference Series, Automation of the OAN/SPM 1.5-meter Johnson telescope for operations with RATIR

Webbink R. F., 1984, ApJ, 277, 355

Whelan J., Iben Jr. I., 1973, ApJ, 186, 1007

Woosley S. E., Weaver T. A., 1994, ApJ, 423, 371

Yaron O., Gal-Yam A., 2012, PASP, 124, 668

Yu C., Modjaz M., Li W. D., 2000, IAU Circ., 7458, 1